

LooseCut: Interactive Image Segmentation with Loosely Bounded Boxes

Hongkai Yu[†], Youjie Zhou[†], Hui Qian[‡], Min Xian^{*}, Yuewei Lin[†], Dazhou Guo[†], Kang Zheng[†],
Kareem Abdelfatah[†] and Song Wang[†]

[†]Department of Computer Science & Engineering, University of South Carolina, Columbia, SC 29208

[‡]College of Computer Science, Zhejiang University, Hangzhou, China

^{*}Department of Computer Science, Utah State University, Logan, UT 84341

{yu55, zhou42}@email.sc.edu, qianhui@zju.edu.cn, min.xian@aggiemail.usu.edu,
{lin59, guo22, zheng37}@email.sc.edu, ker00@fayoum.edu.eg and songwang@cec.sc.edu

Abstract

One popular approach to interactively segment the foreground object of interest from an image is to annotate a bounding box that covers the foreground object. This input bounding box facilitates the estimation of the appearance models of the foreground and background, with which a binary labeling is finally performed to achieve a refined segmentation. One major issue of the existing algorithms for such interactive image segmentation, including the widely used GrabCut, is their preference of an input bounding box that tightly encloses the foreground object. This increases the annotation burden, and prevents these algorithms from utilizing automatically detected bounding boxes. In this paper, we develop a new LooseCut algorithm that can handle cases where the input bounding box only loosely covers the foreground object. We propose a new Markov Random Fields (MRF) based segmentation energy function, including a global energy term to better distinguish the foreground and background, and a high-order energy term to encourage the label spatial consistency. This MRF energy function is then minimized by an iterated max-flow algorithm. In the experiments, we evaluate LooseCut in three publicly-available image datasets, and compare its performance against several state-of-the-art interactive image segmentation algorithms. We also show that LooseCut can be used for enhancing the performance of unsupervised video segmentation and image-based saliency detection.

1. Introduction

Accurately segmenting a foreground object of interest from an image with convenient human interactions plays a central role in image and video editing. One widely used interaction is to annotate a bounding box around the fore-

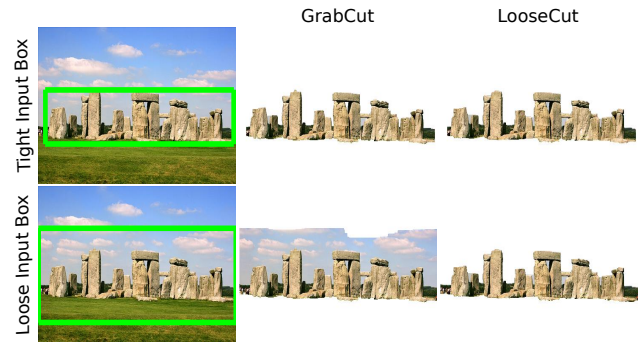


Figure 1. Sample results from GrabCut and the proposed LooseCut with tightly and loosely bounded boxes.

ground object. On one hand, this input bounding box provides the spatial location of the foreground. On the other hand, based on the image information within and outside this bounding box, we can have an initial estimation of the appearance models of the foreground and background, with which a binary labeling is finally performed to achieve a refined segmentation of the foreground and background [15, 17, 16, 18, 13, 10].

However, due to the complexity of the object boundary and appearance, most existing methods of this kind prefer the input bounding box to tightly enclose the foreground object. An example is shown in Fig. 1, where the widely used GrabCut [15] algorithm fails when the bounding box does not tightly cover the foreground object. The preference of a tight bounding box increases the burden of the human interaction, and moreover it prevents these algorithms from utilizing automatically generated bounding boxes, such as boxes from object proposals [2, 23, 22], that are usually not guaranteed to tightly cover the foreground object. In this paper, we focus on developing a new LooseCut algorithm that can accurately segment the foreground object with loosely-

bounded boxes.

Based on a loosely bounded box, one main problem is that we could not make a reasonable initial estimation of the appearance model of the foreground. In LooseCut, we address this problem by emphasizing the appearance difference between the foreground and background. In particular, we follow GrabCut by formulating the foreground/background segmentation as a binary labeling over a Markov Random Field (MRF) built upon the image grid, and the appearances of the foreground and background are described by two Gaussian Mixture Models (GMMs). To handle the loosely bounded box, we introduce a new global term to the MRF energy such that the similarity between the foreground and background GMMs is minimized. In addition, we introduce a new high-order term to the MRF energy to enable the correct labeling of the background pixels within the bounding box. The proposed MRF energy function is then minimized by an iterated max-flow algorithm.

The remainder of the paper is organized as follows. Section 2 reviews the related work. Section 3.1 briefly reviews the GrabCut algorithm. Section 3.2 describes the proposed LooseCut algorithm in detail. Section 4 reports the experimental results, followed by a briefly conclusion in Section 5.

2. Related Work

In recent years, interactive image segmentation based on input bounding boxes have drawn much attention in the computer vision and graphics community, resulting in a number of effective algorithms [15, 17, 16, 18, 13, 10]. Starting from the classical GrabCut algorithm, many of these algorithms use graph cut models: the input image is modeled by a graph and the foreground/background segmentation is then modeled by a binary graph cut that minimizes a pre-defined energy function [6]. In GrabCut [15], initial appearance models of the foreground and background are estimated using the image information within and outside the bounding box. A binary MRF model is then applied to label each pixel as the foreground or background, based on which the appearance models of the foreground and background are re-estimated. This process is repeated until convergence. As illustrated in Fig. 1, the performance of GrabCut is highly dependent on the initial estimation of the appearance models of the foreground and background, which might be very poor when the input bounding box does not tightly cover the foreground object. The LooseCut algorithm developed in this paper also follows the general procedure introduced in GrabCut, but introducing new terms to the MRF energy to specifically handle the loosely-bounded boxes. In Section 3.1, we will briefly review the GrabCut algorithm before introducing the proposed LooseCut algorithm.

PinPoint [13] is another MRF-based algorithm for inter-

active image segmentation with a bounding box. It incorporates a topology prior derived from geometry properties of the bounding box and encourages the segmented foreground to be tightly enclosed by the bounding box. Therefore, its performance gets much worse with a loosely bounded box. OneCut [17] is another recently developed algorithm using the MRF model for interactive image segmentation. Similar to our proposed LooseCut algorithm, OneCut also incorporates an MRF energy term that reflects the dissimilarity between the foreground and the background. As shown in the latter experiments, the L_1 -distance based dissimilarity measure used in OneCut is still insufficient to handle loosely-bounded boxes. In fact, with loosely bounded boxes, the performance of OneCut is even not as good as the original GrabCut. In [16], a pPBC algorithm is developed for interactive image segmentation using an efficient parametric pseudo-bound optimization strategy. However, pPBC tends to converge to a local minimum in optimizing the energy function when the input bounding box is loose. In Section 4, we also include pPBC as a comparison method in experiments.

Other than using the MRF model, MILCut [18] formulates the interactive image segmentation as a multiple instance learning problem by generating positive bags along the sweeping lines within the bounding box. Within a loosely-bounded box, MILCut may not generate the desirable positive bags along the sweeping lines. Active contour [10] takes the input bounding box as an initial contour and iteratively deforms it toward the boundary of the foreground object. Due to its sensitivity to image noise, active contour usually requires the initial contour to be close to the underlying foreground object boundary.

3. Proposed Approach

In this section, we first review the GrabCut algorithm, based on which we then develop the proposed LooseCut algorithm.

3.1. GrabCut

GrabCut [15] actually performs a binary labeling to each pixel using an MRF model. Let $X = \{x_i\}_{i=1}^n$ be the binary labels at each pixel i , where $x_i = 1$ if i is in foreground $x_i = 0$ if i is in background. We seek an optimal labeling that minimizes

$$E_{GC}(X) = \sum_i D(x_i) + \sum_{i,j \in \mathcal{N}} V(x_i, x_j), \quad (1)$$

where \mathcal{N} defines a pixel neighboring system, e.g., 4-neighbor or 8-neighbor connectivity. The unary term $D(x_i)$ measures the cost of labeling pixel i as foreground or background. The pairwise term $V(x_i, x_j)$ enables the smoothness of the labels by penalizing different labels to neigh-

boring pixels. Max-flow algorithm [6] is usually used for solving this MRF optimization problem.

As an interactive image segmentation algorithm, GrabCut takes the following steps to achieve the binary image segmentation with an input bounding box:

1. Building two GMMs as initial estimations of the models of the foreground and background appearances, using the pixels inside and outside the bounding box respectively.
2. Based on these two GMMs, quantizing the foreground and background likelihood of each pixel and using it to define the unary term $D(x_i)$.
3. Solving for the optimal labeling that minimizes Eq. (1).
4. Based on the obtained labeling, refining the foreground and background GMMs and going back to Step 2. Repeating this process until convergence.

As mentioned earlier, with a loosely-bounded box, the initial GMMs constructed in Step 1 cannot well describe the foreground appearance and leads to under-segmentation of the foreground as shown in Fig. 1.

3.2. Energy function for LooseCut

Following the MRF model used in GrabCut, we propose a new energy function for LooseCut as

$$E(X) = E_{GC}(X) + E_G(X) + \beta E_H(X), \quad (2)$$

where E_{GC} is the original MRF energy function shown in Eq. (1), E_G is a new global energy term highlighting the dissimilarity between the constructed foreground and background GMMs, and E_H is a high-order MRF term that encourages pixels with similar features to be assigned a same label even if they are not neighboring to each other. The parameter $\beta > 0$ weights the high-order energy term.

By including the term E_G , the resulting binary labeling emphasizes the difference between the foreground and background and is less sensitive to the inaccuracy of the foreground and background appearance models initially estimated from a loosely-bounded box. By including the high-order term E_H , background pixels within the loosely-bounded box are more likely to be labeled correctly as background, by associating to distant background pixels outside the bounding box. We expect the inclusion of these two terms in the MRF energy can help improve the performance of the interactive image segmentation with loosely-bounded boxes. In the following, we elaborate on the design of these two terms.

3.3. Definition of the Term E_G

Let $M_f(X)$ and $M_b(X)$ be the GMMs of the foreground and background resulting from the binary labeling X , respectively. For simplicity, we may ignore the variable X in these two GMM notations when it does not lead to any ambiguity. M_f has K_f Gaussian components M_f^i with means μ_f^i and weights π_f^i , $i = 1, 2, \dots, K_f$ and M_b has K_b Gaussian components M_b^j with means μ_b^j and weights π_b^j , $j = 1, 2, \dots, K_b$. For each Gaussian component M_f^i in the foreground GMM M_f , we first find its nearest Gaussian component $M_b^{j(i)}$ in M_b as

$$j(i) = \arg \min_{j \in \{1, \dots, K_b\}} |\mu_f^i - \mu_b^j|. \quad (3)$$

With this we can define the similarity between the Gaussian component M_f^i and the entire background GMM M_b as

$$S(M_f^i, M_b) = \frac{1}{\pi_f^i |\mu_f^i - \mu_b^{j(i)}|}, \quad (4)$$

which is the (weighted) inverse of the mean difference between M_f^i and its nearest Gaussian component in the background GMM. Similar definition of GMM distance can be found in [19]. Based on this similarity, we define the global term E_G as

$$E_G(X) = \sum_{i=1}^{K_f} S(M_f^i, M_b). \quad (5)$$

3.4. Definition of the High-Order Term E_H

As mentioned earlier, the goal of introducing the high-order term E_H is to associate distant pixels with similar features. To achieve this goal, we first cluster all the image pixels such that pixels with similar features are grouped into the same cluster. In this paper, we use a recent superpixel algorithm [21] that considers both within-cluster feature consistency and the cluster-boundary smoothness for pixel clustering. Following a K-means-style procedure, this clustering algorithm partitions the image into a set of compact superpixels and each resulting cluster is made up of one or more superpixels. An example is shown in Fig. 2, where the region color indicates the clusters: superpixels with the same color constitute a cluster.

Based on the clusters, we define the high-order term as

$$E_H(\mathbf{X}) = \sum_k \sum_{i,j \in C_k} \phi(x_i \neq x_j), \quad (6)$$

where C_k indicates the cluster k and $\phi(\cdot)$ is an indicator function. With this term, the proposed MRF model is biased to assign a same label to the pixels within a cluster even if they are not near to each other. An example is shown in

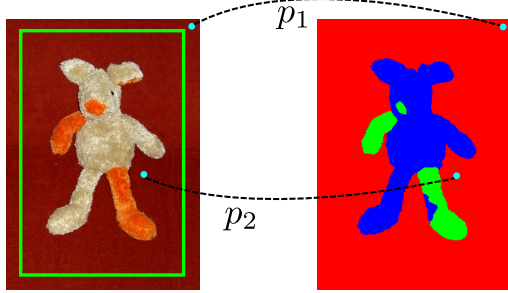


Figure 2. An illustration of the pixel clusters and the definition of the high-order term E_H .

Fig. 2, where p_1 and p_2 are two distant pixels – one is located inside the bounding box and the other is located outside the bounding box. However, both of them are from background and show similar image features. By grouping them into a same cluster, the proposed algorithm may still choose to assign them a same label, i.e., background, in the final segmentation due to the inclusion of the term E_H .

3.5. Optimization

In this section, we propose an algorithm to find the optimal binary labeling that minimizes the energy function $E(X)$ defined in Eq. (2). We can divide $E(X)$ into two components as $E(X) = E_C(X) + E_G(X)$ where $E_C(X) = E_{GC}(X) + \beta E_H(X)$. It is easy to see that $E_C(X)$ is a classical MRF energy function with a high-order term and it can be optimized using many efficient algorithms, such as max-flow/min-cut algorithm. However, the global term $E_G(X)$ involves the region statistical information and it is nontrivial to be integrated into the unary and binary MRF terms for an optimization.

In this paper, we propose an algorithm to optimize these two components alternately. Specifically, we introduce the foreground/background GMMs (M_f, M_b) as the intermediate variables and rewrite the two components as $E_C(X|(M_f, M_b))$ and $E_G((M_f, M_b)|X)$. In our iterative optimization algorithm, we first fix the labeling X and find GMMs (M_f, M_b) to optimize the component $E_G((M_f, M_b)|X)$ and then fix the GMMs (M_f, M_b) to optimize $E_C(X|(M_f, M_b))$. We repeatedly these two optimization steps alternately until convergence to achieve the optimal labeling X and the final foreground/background segmentation. In the following, we elaborate on these two optimization steps.

Optimizing $E_G((M_f, M_b)|X)$: With the current binary labeling X , we can estimate the foreground and background GMMs (M_f, M_b) using a standard EM-based clustering algorithm. At the very first step, we construct an initial binary labeling directly using the input bounding box: pixels inside the bounding box are labeled foreground and pixels

outside the bounding box are labeled background. Within each iteration, we take the binary labeling X obtained from the previous step of optimizing $E_C(X|(M_f, M_b))$ for constructing (M_f, M_b) .

However, (M_f, M_b) estimated using a standard clustering algorithm does not consider to minimize the global term $E_G((M_f, M_b)|X)$. In this section, we propose additional operations to address this problem. In particular, we know that the estimated background M_b is usually more credible since all the pixels outside the bounding box are known to be in the background. However, the estimated foreground GMM M_f is less credible because many pixels labeled as foreground may still come from background, especially in the early iterations. For example, at the very first step, we take all the pixels in a loosely bounded box to estimate M_f and such a box may contain a large number of background pixels.

Therefore, in this step of optimization, we take (M_f, M_b) estimated using standard EM algorithm, keep the background GMM M_b , but further update M_f to minimize E_G . For this purpose, in EM clustering, we intentionally make M_f to have K more Gaussian components than M_b . In the latter experiments, we simply set $K = 1$. We then calculate the similarity $S(M_f^i, M_b)$ between each Gaussian component of M_f and the GMM M_b , by following Eq. (4) and identify the K Gaussian components of M_f with the largest similarity to M_b . Among these K components, if any one, say M_f^i , satisfies $S(M_f^i, M_b) > \delta$, we delete it from M_f . After the deletion, we use the remaining Gaussian components to construct an updated M_f . This update operation helps exclude the background pixels from estimating the foreground GMM M_f and always decreases $E_G((M_f, M_b)|X)$.

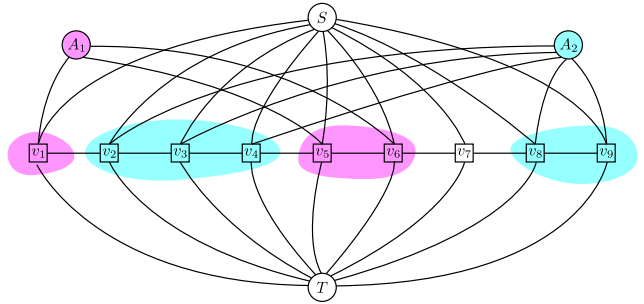


Figure 3. Graph construction for optimization. Nodes/pixels in image belonging to the same cluster are connected to the same auxiliary node. Only two clusters are shown in this figure. Best view in color.

Optimizing $E_C(X|(M_f, M_b))$: Inspired by [11] and [17], we build an undirect graph for modeling the MRF energy E_C . As shown in Fig. 3, each pixel is represented by a node. As discussed earlier, i.e., Eq. (6), the higher-order term E_H is defined between pixels within pixel clusters ob-

tained by a superpixel algorithm [21]. For each pixel cluster, we construct an auxiliary node in the graph, as shown by nodes A_1 and A_2 in Fig. 3, where pixel nodes v_i 's in different clusters are shown in different colors. The edge weight between a pixel node and its corresponding auxiliary node is set to 1. With these cluster-specific auxiliary nodes, assigning pixels from the same cluster with different labels always increases the high-order energy E_H . Following [17], we use the max-flow algorithm [6] on the constructed graph to seek an optimal binary labeling X that minimizes the energy $E_C(X|(M_f, M_b))$. The GMMs (M_f, M_b) obtained from the previous step of optimizing E_G are taken to define the unary term in E_C .

The full LooseCut algorithm can be summarized as follows:

Algorithm 1 LooseCut

Input: Image I , Bounding box B , # of pixel clusters N

Output: Binary labeling X to pixels in I

- 1: Construct N pixel clusters using algorithm [21].
- 2: Create initial labeling X using box B .
- 3: **repeat**
- 4: Based on the current labeling X , estimate and update GMMs (M_f, M_b) by optimizing E_G .
- 5: Construct the graph using the updated (M_f, M_b) with N auxiliary nodes as shown in Fig. 3.
- 6: Apply the max-flow algorithm [6] to update labeling X by minimizing E_C .
- 7: **until** Convergence or maximum iterations reached

4. Experiments

To justify the proposed LooseCut algorithm, we conduct experiments on three widely used image datasets – the GrabCut dataset [15], the Weizmann dataset [3, 5], and the iCoseg dataset [4], and compare its performance against several state-of-the-art interactive image segmentation methods, including GrabCut [15], OneCut [17], MIL-Cut [18], and pPBC [16]. We also conduct experiments to show the effectiveness of LooseCut in two applications: unsupervised video segmentation and image saliency detection.

Metrics: As in [18] [17] [13], we use *Error Rate* to evaluate an interactive image segmentation by counting the percentage of misclassified pixels inside the bounding box. We also take the pixel-wise *F-measure* as an evaluation metric, which combines the precision and recall metrics in terms of the ground-truth segmentation.

Parameter Settings: For the number of Gaussian components in GMMs, M_b always has 5 components. As described in Section 3.5, M_f has 6 and 5 components before and after optimizing E_H . The number of pixel clus-

ters (auxiliary nodes in graph) is set to $N = 16$. For the LooseCut energy defined in Eq. (2), we consistently set $\beta = 0.01$. The unary term and binary term in Eq. (2) are the same as in [15] and RGB color features are used to construct the GMMs. We set $\delta = 0.2$ in optimizing the $E_G((M_f, M_b)|X)$. For all the comparison methods, we follow their default or recommended settings.

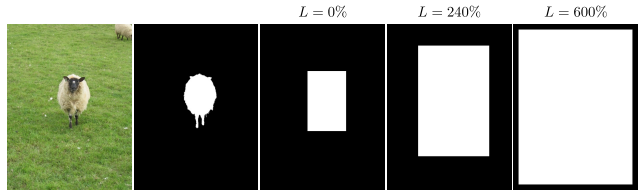


Figure 4. Bounding boxes with different looseness. From left to right are the image, the ground-truth foreground, the baseline bounding box and a series of bounding boxes with increased looseness.

4.1. Interactive Image Segmentation

In this experiment, we construct bounding boxes with different looseness and examine the resulting segmentation. As illustrated in Fig. 4, we compute the fit box to the ground-truth foreground and slightly dilate it by 10 pixels along four directions, i.e., left, right, up, and down. We take it as the baseline bounding box with 0% looseness. We then keep dilating this bounding box uniformly along all four directions to generate a series of looser bounding boxes – a box with a looseness L (in percentage) indicates its area increase by L against the baseline bounding box. A bounding box will be cropped when any of its sides reaches the image perimeter. An example is shown in Fig. 4.

GrabCut dataset [15] consists of 50 images. Nine of them contain multiple objects while the ground truth is only annotated on a single object. Such images are not applicable for testing the loosely bounded boxes because a loosely bounded box may cover other objects. Therefore, we use the remaining 41 images in our experiments. From Weizmann dataset [3, 5], we pick a subset of 45 images for testing, by discarding the images where the baseline bounding box has almost cover the full image and cannot be dilated to construct looser bounding boxes. For the similar reason, from iCoseg dataset [4], we select a subset of 45 images for our experiment.

Experimental results on these three datasets are summarized in Fig. 5. In general, the segmentation performance degrades when the bounding-box looseness increases for both the proposed LooseCut and all the comparison methods. However, LooseCut shows a slower performance degradation than the comparison methods. When the looseness is high, e.g., $L = 300\%$ or $L = 600\%$, LooseCut shows much higher F-measure and much lower Error Rate

| Methods | $L = 0\%$ | | $L = 120\%$ | | $L = 240\%$ | | $L = 600\%$ | |
|----------|--------------|------------|--------------|------------|--------------|------------|--------------|------------|
| | F-measure | Error Rate |
| GrabCut | 0.916 | 7.4 | 0.858 | 10.1 | 0.816 | 12.6 | 0.788 | 13.7 |
| OneCut | 0.923 | 6.6 | 0.853 | 8.7 | 0.785 | 9.9 | 0.706 | 13.7 |
| pPBC | 0.910 | 7.5 | 0.844 | 9.1 | 0.827 | 9.4 | 0.783 | 12.3 |
| MILCut | - | 3.6 | - | - | - | - | - | - |
| LooseCut | 0.882 | 7.9 | 0.867 | 5.8 | 0.844 | 6.9 | 0.826 | 6.8 |

Table 1. Segmentation performance on GrabCut dataset with bounding boxes of different looseness.

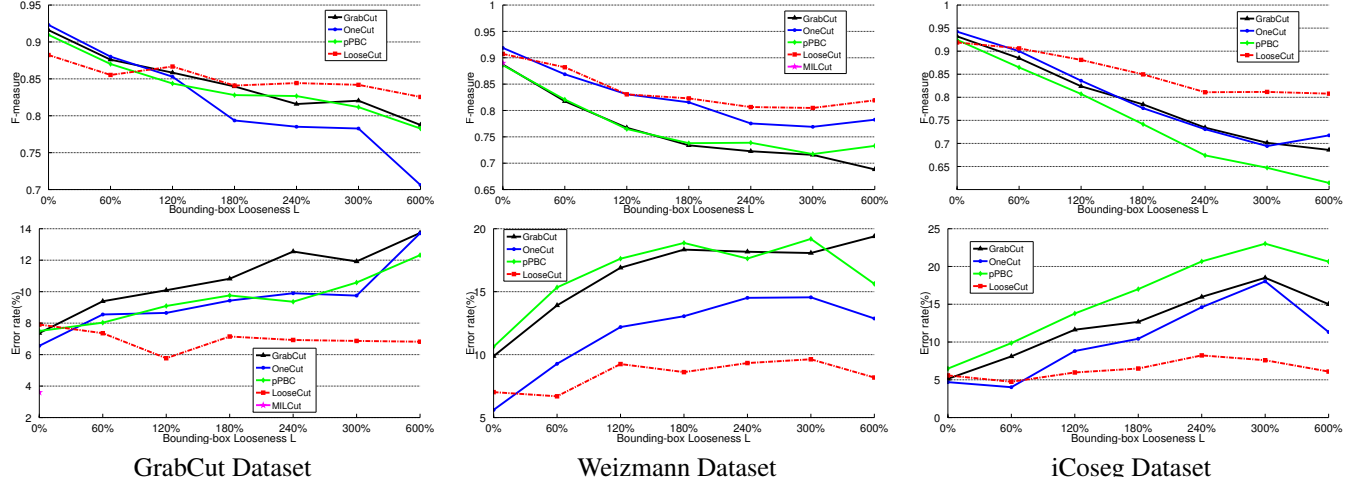


Figure 5. Interactive image segmentation performance (top: F-measure; bottom: Error Rate) on three widely used datasets.

than all the comparison methods. Since MILCut’s code is not publicly available, we only report MILCut’s F-measure and Error Rate values with the baseline bounding boxes on the GrabCut dataset and the Weizmann dataset by copying it from the original paper. Table 1 reports the values of F-measure and Error Rate of segmentation with varying-looseness bounding boxes on GrabCut dataset. Sample segmentation results, together with the input bounding boxes with different looseness, are shown in Fig. 6.

4.2. Unsupervised Video Segmentation

The goal of unsupervised video segmentation is to automatically segment the objects of interest from each video frame. The segmented objects can then be associated across frames to infer the motion and action of these objects. It is of fundamental importance for video analysis and semantic video understanding [8]. One popular approach for unsupervised video segmentation is to detect a set of object proposals, in the form of bounding boxes [12], from each frame and then extract the objects of interest from these proposals [20].

In practice, because the object-proposal algorithm does not consider object category information, a detected proposal may only cover part of the object of interest or even show no overlap with the object of interest. To address this issue, we can detect a set of object proposals and merge them together to construct a large mask (not necessarily

| Methods | F-measure | Error Rate |
|-------------------------|-------------|-------------|
| FusionEdgeBox Mask Only | 0.35 | 77.0 |
| GrabCut | 0.55 | 30.5 |
| OneCut | 0.58 | 25.1 |
| pPBC | 0.54 | 31.6 |
| LooseCut | 0.64 | 17.0 |

Table 2. Video segmentation performance on JHMDB video dataset.

a rectangle box), which has a better chance to cover the whole object. Clearly, this merged mask may only loosely bound the object of interest and in this experiment, we apply LooseCut for object segmentation based on this merged mask. Specifically, we apply a recent FusionEdgeBox algorithm [22] to detect 10 object proposals in each video frame for the merged mask.

This experiment is conducted on the JHMDB video dataset [9], which consists of videos for 21 classes of actions. We select one video from each class, and in total 21 videos, 657 frames, for our experiment. Table 2 shows the unsupervised video segmentation performance, in terms of F-measure and Error Rate averaged over all the frames, on these 21 videos. We can see that the proposed LooseCut substantially outperforms GrabCut, OneCut and pPBC in this task. Sample video segmentation results are shown in Fig. 7.



Figure 6. Sample results for interactive image segmentation.

| Methods | Precision | Recall | F-measure |
|----------|-------------|-------------|-------------|
| FT [1] | 0.75 | 0.57 | 0.61 |
| RC [7] | 0.86 | 0.85 | 0.84 |
| GrabCut | 0.85 | 0.61 | 0.67 |
| OneCut | 0.86 | 0.76 | 0.77 |
| pPBC | 0.84 | 0.66 | 0.69 |
| LooseCut | 0.84 | 0.78 | 0.78 |

Table 3. Performance of saliency detection on the Salient Object dataset.

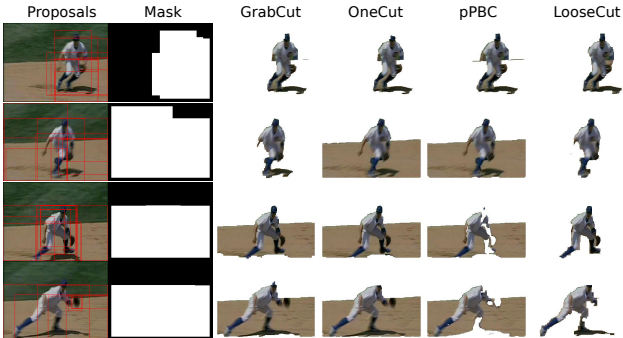


Figure 7. Sample video segmentation results on JHMDB video dataset. From left to right are: top 10 detected object proposals (shown in red rectangles), merged mask and the segmentation results using GrabCut, OneCut, pPBC, and LooseCut, respectively.

4.3. Image Saliency Detection

Recently, GrabCut has been used to detect the salient area from an image [14]. As illustrated in Fig. 8: a set of pre-defined bounding boxes are overlaid to the input image and with each bounding box, GrabCut is applied for a foreground segmentation. The probabilistic saliency map is finally constructed by combining all the foreground segmentations. In this experiment, we show that, by using LooseCut instead of GrabCut, we can achieve better saliency detection.

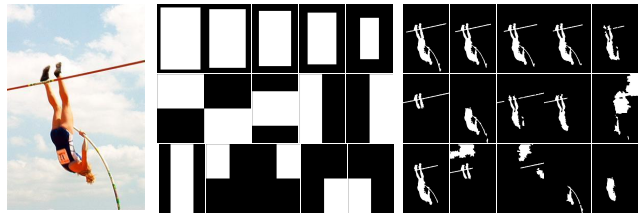


Figure 8. 15 pre-defined masks for saliency detection (middle), and their corresponding segmentation results using LooseCut (right).

In this experiment, out of 1000 images in the Salient Object dataset [1], we randomly select 100 images for testing. 15 pre-defined masks are shown in Fig. 8. For quantitative evaluation, we follow [1] to binarize a resulting saliency map using an adaptive threshold, which is set to be two

| Methods | Weizmann Dataset | | Saliency Detection | |
|-----------|------------------|------------|--------------------|------------|
| | F-measure | Error Rate | F-measure | Error Rate |
| w/o E_H | 0.875 | 7.9 | 0.759 | - |
| w/ E_H | 0.879 | 7.4 | 0.780 | - |

Table 4. Performance of LooseCut with and without the high-order term E_H . Note that Error Rate (%) metric is not applicable to saliency detection.

times the mean saliency of the map. Table 3 reports the precision, recall and F-measure of saliency detection when using GrabCut, OneCut, pPBC, and the proposed LooseCut for foreground segmentation. We also include comparisons of two state-of-the-art saliency detection methods that do not use pre-defined masks, namely FT [1] and RC [7]. Sample saliency detection results are shown in Fig. 9.

We can see that LooseCut clearly outperforms GrabCut, OneCut and pPBC in this task. It also outperforms FT which does not use bounding-box based segmentation. RC [7] achieves the best performance for saliency detection, because it combines the global region contrast and spatial information that contain more cues than the above mentioned approaches of combining multiple foreground segmentations with multiple pre-defined bounding boxes.

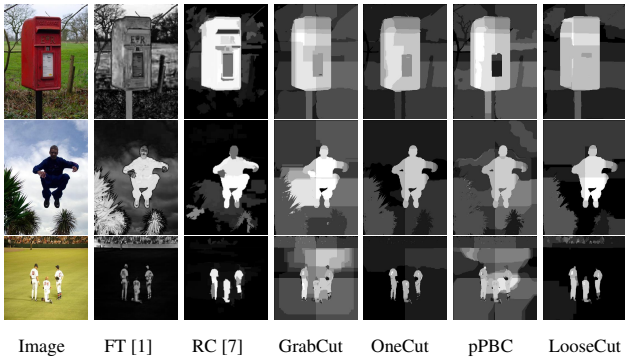


Figure 9. Sample saliency detection results.

4.4. Additional Results

In this section, we report additional results that justify the usefulness of the high-order term E_H , the running time of proposed algorithm and possible failure cases.

To justify the usefulness of the high-order term E_H , we run experiments on the Weizmann dataset and Saliency Detection dataset by removing the term E_H and its corresponding optimization step in the proposed LooseCut algorithm. The quantitative performance is shown in Table 4. We can see that, by including the high-order term E_H , LooseCut performs better image segmentation and saliency detection. Sample results are shown in Fig. 10.

For the running time, we test LooseCut and all the comparison methods on a PC with Intel 3.3GHz CPU and 4GB

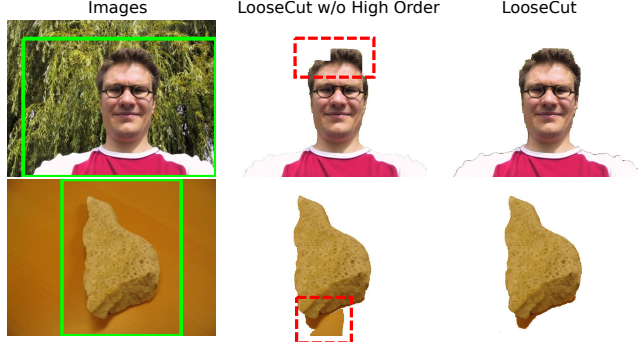


Figure 10. The effects of high-order energy in LooseCut. Our high-order energy encourages pixels with similar feature to be assigned same labels.

| Methods | 64*64 | 128*128 | 256*256 | 512*512 | 1024*1024 |
|----------|-------|---------|---------|---------|-----------|
| GrabCut | 0.16 | 0.28 | 1.47 | 3.81 | 25.21 |
| OneCut | 0.03 | 0.09 | 0.49 | 5.72 | 77.80 |
| pPBC | 0.14 | 0.37 | 2.70 | 26.14 | 305.60 |
| LooseCut | 0.32 | 0.43 | 1.68 | 7.63 | 66.52 |

Table 5. Running time (in seconds) with increasing image size.

RAM. We compares their running time for different image size. In this experiment, OneCut only has one iteration, and the iterations of GrabCut and LooseCut are stopped until convergence or a maximum 10 iterations is reached. As shown in Table 5, if the image size is less than 512×512 , the running time of three algorithms are very close. For large images, LooseCut and OneCut takes more time than GrabCut. In general, LooseCut still shows reasonable running time. Our current LooseCut code is implemented in Matlab and C++, and it can be substantially optimized for speed.

By including a global term E_G that emphasizes the appearance difference between foreground and background, LooseCut may fail when the foreground and background show similar appearances. Failure cases are shown in Fig. 11, where the foreground object shows similar colors and texture to the background. LooseCut cannot distinguish them and produces an undesired fragmented segmentation.



Figure 11. Failure cases of LooseCut.

5. Conclusion

This paper proposed a new LooseCut algorithm for interactive image segmentation by taking a loosely bounded box. Extended from the GrabCut energy, we further introduced a global energy term to emphasize the appearance

difference between the foreground and the background and a high-order energy term to associate the background pixels inside and outside the bounding box. We developed an iterative algorithm to optimize the new energy function. Experiments on three image segmentation datasets showed the effectiveness of *LooseCut* against several state-of-the-art algorithms. We also showed that *LooseCut* can be used for enhance the important applications of unsupervised video segmentation and image saliency detection.

References

- [1] R. Achanta, S. Hemami, F. Estrada, and S. Sussstrunk. Frequency-tuned salient region detection. In *CVPR*, pages 1597–1604, 2009.
- [2] B. Alexe, T. Deselaers, and V. Ferrari. What is an object? In *CVPR*, pages 73–80, 2010.
- [3] S. Alpert, M. Galun, R. Basri, and A. Brandt. Image segmentation by probabilistic bottom-up aggregation and cue integration. In *CVPR*, pages 1–8, 2007.
- [4] D. Batra, A. Kowdle, D. Parikh, J. Luo, and T. Chen. icoseg: Interactive co-segmentation with intelligent scribble guidance. In *CVPR*, pages 3169–3176, 2010.
- [5] E. Borenstein and S. Ullman. Class-specific, top-down segmentation. In *ECCV*, pages 109–122. 2002.
- [6] Y. Boykov and M.-P. Jolly. Interactive graph cuts for optimal boundary & region segmentation of objects in nd images. In *ICCV*, pages 105–112, 2001.
- [7] M.-M. Cheng, N. Mitra, X. Huang, P. Torr, and S.-M. Hu. Global contrast based salient region detection. *TPAMI*, 37(3):569–582, 2015.
- [8] M. Grundmann, V. Kwatra, M. Han, and I. Essa. Efficient hierarchical graph-based video segmentation. In *CVPR*, pages 2141–2148, 2010.
- [9] H. Jhuang, J. Gall, S. Zuffi, C. Schmid, and M. J. Black. Towards understanding action recognition. In *ICCV*, pages 3192–3199, 2013.
- [10] M. Kass, A. Witkin, and D. Terzopoulos. Snakes: Active contour models. *IJCV*, 1(4):321–331, 1988.
- [11] P. Kohli, L. Ladicky, and P. Torr. Robust higher order potentials for enforcing label consistency. *IJCV*, 82(3):302–324, 2009.
- [12] Y. Lee, J. Kim, and K. Grauman. Key-segments for video object segmentation. In *ICCV*, pages 1995–2002, 2011.
- [13] V. Lempitsky, P. Kohli, C. Rother, and T. Sharp. Image segmentation with a bounding box prior. In *ICCV*, pages 277–284, 2009.
- [14] H. Li, F. Meng, and K. Ngan. Co-salient object detection from multiple images. *TMM*, 15(8):1896–1909, 2013.
- [15] C. Rother, V. Kolmogorov, and A. Blake. Grabcut: Interactive foreground extraction using iterated graph cuts. *ACM Transactions on Graphics*, 23(3):309–314, 2004.
- [16] M. Tang, I. Ayed, and Y. Boykov. Pseudo-bound optimization for binary energies. In *ECCV*, pages 691–707, 2014.
- [17] M. Tang, L. Gorelick, O. Veksler, and Y. Boykov. Grabcut in one cut. In *ICCV*, pages 1769–1776, 2013.
- [18] J. Wu, Y. Zhao, J.-Y. Zhu, S. Luo, and Z. Tu. Milcut: A sweeping line multiple instance learning paradigm for interactive image segmentation. In *CVPR*, pages 256–263, 2014.
- [19] H. Yu, M. Xian, and X. Qi. Unsupervised co-segmentation based on a new global gmm constraint in mrf. In *ICIP*, pages 4412–4416, 2014.
- [20] D. Zhang, O. Javed, and M. Shah. Video object co-segmentation by regulated maximum weight cliques. In *ECCV*, pages 551–566. 2014.
- [21] Y. Zhou, L.Ju, and S. Wang. Multiscale superpixels and supervoxels based on hierarchical edge-weighted centroidal voronoi tessellation. In *WACV*, pages 1076–1083, 2015.
- [22] Y. Zhou, H. Yu, and S. Wang. Feature sampling strategies for action recognition. *CoRR*, abs/1501.06993, 2015.
- [23] C. Zitnick and P. Dollár. Edge boxes: Locating object proposals from edges. In *ECCV*, pages 391–405. 2014.